2-(4-Morpholinothio)benzothiazole as a High-efficiency Corrosion Inhibitor for Copper in 0.5 M H₂SO₄ Solution

Wu Long[*], *Wenwen Xiao, Qingshan Liu, Pengli Ge, Tingting Liang*

SINOPEC Northwest Company of China Petroleum and Chemical Corporation, Urumqi 830011, China
[*]E-mail: 305118621@qq.com

This work developed a benzothiazole derivative named 2-(4-Morpholinothio)benzothiazole (MB) to replace toxic corrosion inhibitors. Based on EIS, Polarization curve, weight loss, SEM, LSCM, Langmuir adsorption, and theoretical calculation, the anti-corrosion ability of MB for copper in 0.5 M H₂SO₄ was explored. It was worth noting that the η value reached 94% when the concentration of MB was 1 mM. The supreme anti-corrosion ability of MB for copper could be attributed to a compact MB film formed on the copper surface. Langmuir adsorption and theoretical calculation appropriately demonstrated the anti-corrosion mechanism of MB film on the copper surface from the thermodynamic and molecular levels. We hope this work can accumulate experience in organic corrosion inhibitor research.

1. INTRODUCTION

Due to its excellent electrical, thermal conductivity, and stability, Copper is widely used in light machinery, construction, and national defense [1, 2]. Therefore, copper is called industrial gold. Compared to steel, copper is more resistant to corrosion. In extreme environments, however, copper can also corrode, such as in acid environments [3]. Effectively inhibiting copper corrosion in acid environments can reduce economic losses and the occurrence of safety accidents. Developing effective techniques to inhibit copper corrosion has great research value and practical significance.

Common anti-corrosion protection techniques include electrochemical protection [4], organic coatings [5-7], optimized metal structures [8], and corrosion inhibitors [9-11]. Among those techniques, corrosion inhibitor has many advantages, such as small dose, low cost, and ease of use [12]. Based on the difference in composition, corrosion inhibitors can be divided into inorganic and organic. Inorganic

corrosion inhibitors include zinc salts, phosphates, cerium salts, chromium salts, and nitrites. However, some inorganic corrosion inhibitors are toxic and not eco-friendly, such as nitrite and chromate [13, 14]. So far, some inorganic corrosion inhibitors have been banned.

Organic inhibitors have many advantages compared to inorganic inhibitors [15-17]. Based on heteroatoms (N, O, S, P), benzene rings, and heterocycles [18-20], organic molecules can adsorb on the metal surface by gaining and losing electrons [21]. Finally, an organic protective film is formed on the metal surface. Qiang investigated the anti-corrosion performance of two tetrazole derivatives for copper in an acid environment [22]. Combining experimental results and theoretical calculations, the authors found that the bridged sulfur atom can significantly improve the anti-corrosion performance of tetrazole derivatives. The highest η value of 5-(Benzylthio)-1H-tetrazole was 99.8%. Tan found that difurfuryl disulfide (DFD) and furfuryl mercaptan (FFM) could reduce the corrosion of copper in sulfuric acid [23]. Combining XPS and molecular dynamics results, the authors explained that DFD and FFM were adsorbed on the copper surface in parallel through the coordination bonds. Despite researchers doing much research on organic corrosion inhibitors, it still possesses research value and practical significance in industrial application.

As shown in Fig.1, 2-(4-Morpholinothio)benzothiazole (MB) is the primary raw material for manufacturing industrial rubber products, such as tires, hoses, rubber shoes, and conveyor belts. The main advantages of MB are that it is cheap and easy to obtain. Since it contains a thiazole ring, benzene ring, and heterocycle (N, O, S), MB has the potential to become a corrosion inhibitor. To our knowledge, no work has been reported on MB as a corrosion inhibitor to inhibit copper corrosion in sulfuric acid. Therefore, we explored the anti-corrosion performance of MB on copper in 0.5 M H_2SO_4 via electrochemical experiments, morphology observations, weight loss, and theoretical calculations. We hope this work can contribute to realizing the industrial application of low-cost, high-efficiency corrosion inhibitors.

2-(4-Morpholinothio)benzothiazole
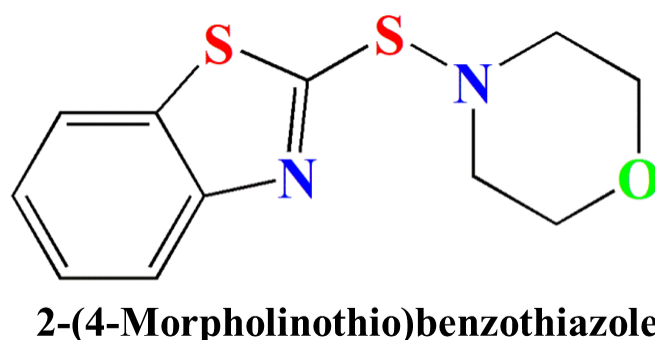
Figure 1. The chemical structure of 2-(4-Morpholinothio)benzothiazole.

2. EXPERIMENTAL

2.1 Materials

Pure copper (99.9 wt%) was purchased at a local dealer, and the sample size for all experiments was 1×1×1 cm^3. The copper working electrode for electrochemical experiments was encapsulated with

epoxy resin, retaining only one surface for test. Before electrochemical testing, the working electrode was polished with sandpaper from 400 to 2000 mesh.

2-(4-Morpholinothio)benzothiazole (MB, Adamas, 97%) was purchased from the Tansoole dealer and used without other purification. Concentrated sulfuric acid (98%) was purchased from the Sinopharm Group. The blank test solution was 0.5 M H_2SO_4, which was obtained by diluting 98% H_2SO_4 with deionized water. The MB concentrations in the test solution were 0.01, 0.1, 0.2, 0.5, and 1 mM.

2.2 Electrochemical test

All electrochemical tests were derived from a three-electrode system that contained a working electrode, a counter electrode (platinum electrode, 2×2 cm^2), and a reference electrode (Saturated Calomel Electrode, SCE). The electrochemical workstation used for the test was CHI 660E, purchased from Shanghai Chenhua Co., Ltd., China. The electrochemical impedance spectroscopy (EIS) test was performed based on the stable open circuit potential. The test frequency range was 10^5 to 10^{-2} Hz, and the disturbance signal was 5 mV. After finishing the EIS test, the polarization curve test was further conducted. Considering that more information can be obtained at a slower scan rate, we chose a scan rate of 1 mV/s. The range of the scan interval was $\pm$ 250 mV based on the open circuit potential. The above tests were performed in a water bath at 25 °C.

2.3 Weight loss

All samples used for the weight loss test were polished from 400 to 5000 mesh, ultrasonic cleaned with deionized water and 97% ethanol, dried with N_2, and weighed with a high-precision electronic balance. Each experiment was performed in triplicate to ensure accurate and reliable data. The pretreated samples were immersed in sulfuric acid solutions containing different concentrations of MB (0, 0.01, 0.1, 0.2, 0.5, and 1 mM) for 8 h. After soaking, the above cleaning and impurity removal work was repeated and weighed again.

2.4 Surface characterization

The copper samples were immersed in 0.5 M H_2SO_4 with and without 1 mM MB for 48 h. Then, they were cleaned and observed via laser scanning confocal microscope (LSCM, Zeiss LSM700) and SEM (FEI Quanta FEG 250). The observation areas in LSCM were 50×50 um^2, and the scale bar in SEM was 50 um.

2.5 Calculation details

The theoretical calculation was executed in this work via Materials Studio (MS) software [24-26]. The molecular structure of MB was geometrically optimized by density functional theory (DFT) using GGA/B3LYP functional with 6-311++G(d,p) basis set [27]. The highest occupied molecular

orbital (HOMO), the lowest unoccupied molecular orbital (LUMO), and relational parameters were obtained and analyzed.

3. RESULTS AND DISCUSSION

3.1 EIS

The EIS curves of various concentrations MB for copper in 0.5 M H_2SO_4 were given in Fig. 2. As shown in Figs. 2a and b, the Nyquist curve of copper in 0.5 M H_2SO_4 solution consisted of an imperfect semicircle in the high-frequency region followed by a straight line in the low-frequency range. The imperfect semicircle was the capacitive arc, indicating the charge transfer on the metal surface [28]. In other words, the smaller radius of the capacitive arc stood for the more easily corroded metal. The straight line was Warburg impedance, indicating dissolved oxygen diffused to the metal surface, or the metal was dissolved in solution [29]. When the MB appeared, it was found that the imperfect semicircle of copper increased. This finding suggested that MB could improve the difficulty of charge transfer on the copper surface. Unfortunately, the EIS curves at low MB concentrations (0.01 to 0.2 mM) still contained Warburg impedance, indicating that MB protective film was relatively loose and could not inhibit the dissolution of copper.
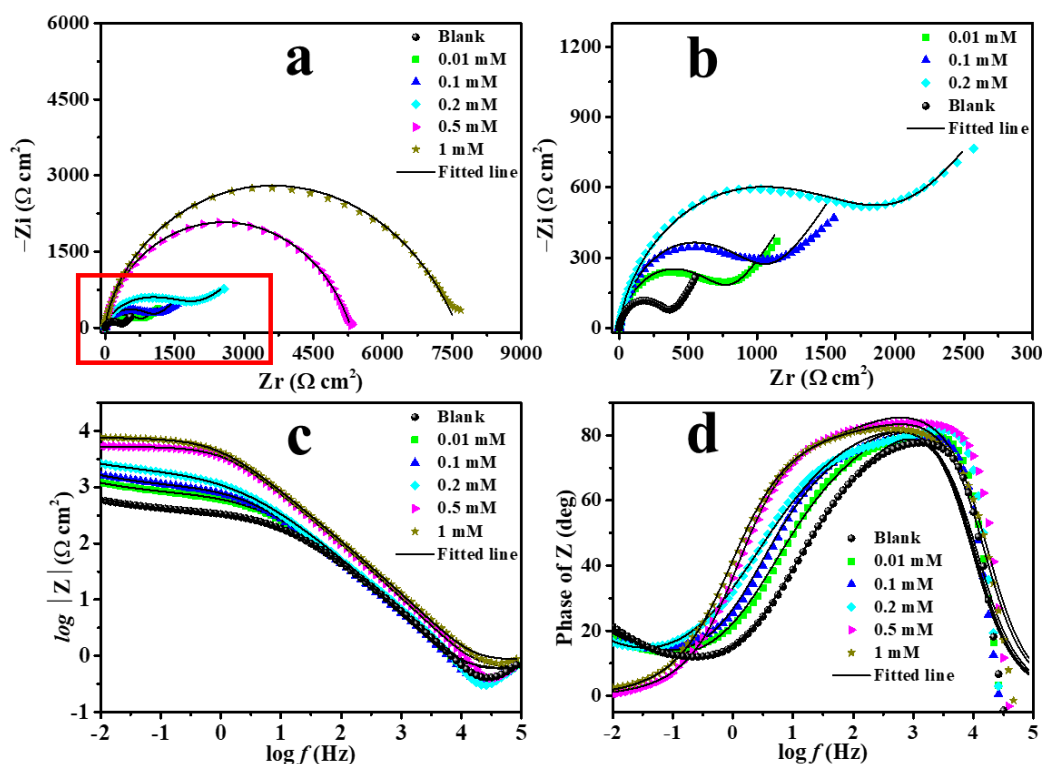
Figure 2. EIS curves recorded for the copper electrode in 0.5 M H_2SO_4 solution containing different concentrations of MB at 298 K, (a) Nyquist plot, (b) Local magnified plot of (a), (c) Bode plot, (d) Phase angle plot.

Fortunately, as the concentration of MB increased to 0.5 mM, the radius of the imperfect semicircle increased significantly, and Warburg impedance also disappeared. This phenomenon showed that a high concentration of MB ($\geq$0.5 mM) could form a compact protective film on the copper surface, thus providing efficient protection for copper. The Bode curves were shown in Fig 2c. The appearance of MB increased the impedance modulus value of copper, and it continued to rise with the increase of the MB concentration. Compared with the blank Bode curve, the impedance modulus value of copper in 1 mM MB solution was improved by more than an order of magnitude. The same situation occurred in the phase angle curves (Fig. 2d), where the presence of MB increased the height and width of the phase angle peak value. This finding also proved that MB could effectively inhibit the corrosion of copper in 0.5 M H_2SO_4.

For quantitative analysis, we fitted the EIS data based on equivalent circuits in Fig. 3. When the concentrations of MB were no more than 0.2 mM, Fig. 3a was used for fitting. In addition, the remaining EIS data were fitted in Fig. 3b. Some key parameters were given in Table 1, such as solution impedance (R_s), film impedance (R_f), charge transfer impedance (R_{ct}), Warburg impedance (W), film capacitance (C_f), and double electrode layer capacitance (C_{dl}). As shown in Table 1, the R_f and R_{ct} values increased with the MB concentrations. Instead, the C_f and C_{dl} values reduced with the MB concentrations. This finding indicated that an MB film was formed on the copper surface and became denser as the MB concentrations increased [30, 31]. The corrosion inhibition efficiency was 94% when the concentration of MB was1 mM, which corresponded to the supreme anti-corrosion property of MB. Compared with the published work [32], higher doses (3 mM) were used to achieve a similar corrosion inhibition efficiency, which further proved the superiority of our work.
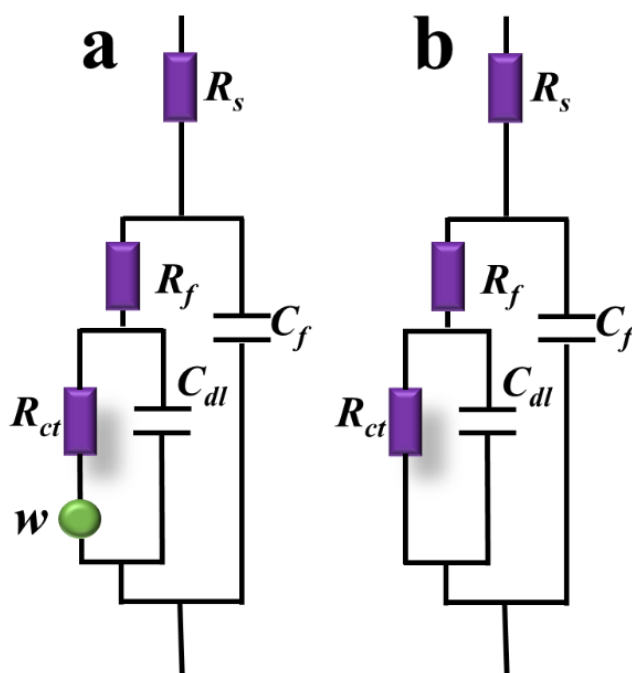

Figure 3. The corresponding equivalent circuits used to fit the EIS experimental data.

Table 1. Impedance parameters for copper in a 0.5 M H_2SO_4 solution in the absence and presence of various concentrations of MB at 298 K.

C (mM)	*R_f* (Ω cm^2)	*R_{ct}* (Ω cm^2)	*C_f* (μF cm^{-2})	*n_1*	*C_{dl}* (μF cm^{-2})	*n_2*	*W* ($\times 10^{-2}\Omega$ cm^2 s$^{1/2}$)	*η* (%)
Blank	40.2	412.5	37.2	1	45.3	0.55	1.35	-
0.01	60.5	751.3	30.1	1	35.4	0.58	0.73	44.2
0.1	63.5	1051.3	24.7	1	26.4	0.61	0.52	59.4
0.2	126.5	2121.9	16.5	1	18.4	0.56	0.43	79.9
0.5	320.9	5089.3	8.7	1	10.3	0.69	-	91.6
1	431.5	7056.9	6.1	1	7.4	0.67	-	94.0

3.2 Polarization curve

The Polarization curve of various concentrations MB for copper in 0.5 M H_2SO_4 was given in Fig. 4. The presence of MB shifted down the copper cathodic and anodic polarization curves, and this phenomenon became more evident with the increase of MB. This finding indicated that MB could reduce the corrosion current density and improve the corrosion resistance of copper. However, the appearance of MB did not affect the shape of Polarization curves, indicating that the copper corrosion mechanism was the same. This conclusion was also confirmed in the other researchers' work [33]. Mainly, a platform was observed in the anodic range (-0.036 V to 0.03 V) when the concentration of MB exceeded 0.2 mM. This platform was attributed to the desorption of MB molecules adsorbed on the copper surface.
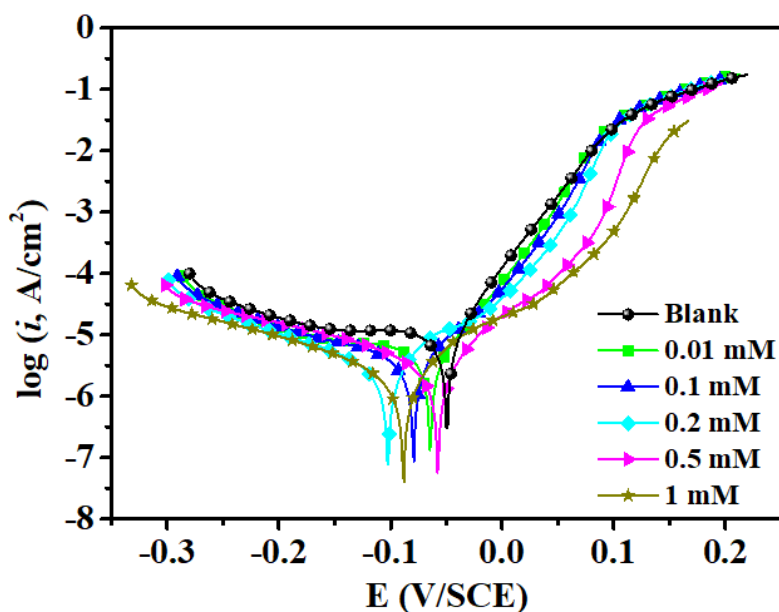
Figure 4. Potentiodynamic polarization curves recorded for the copper electrode in 0.5 M H_2SO_4 solution containing different concentrations of MB at 298 K.
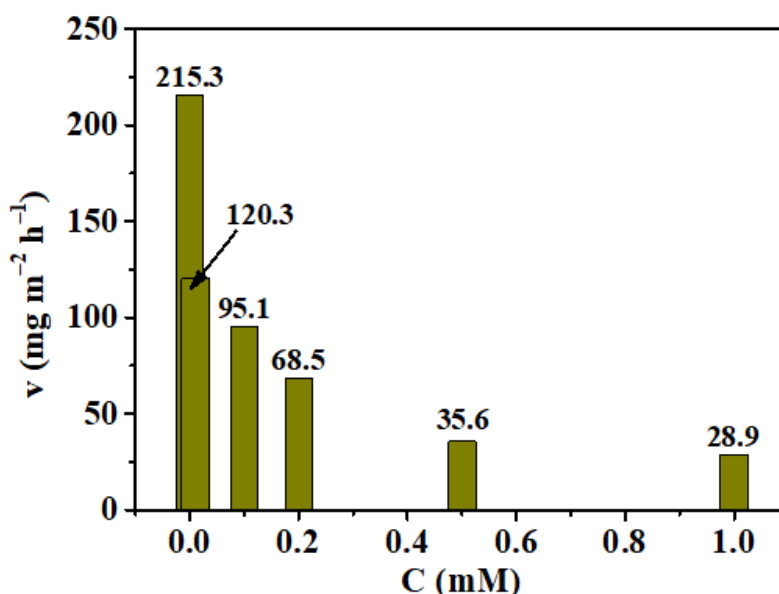
Table 2. Potentiodynamic polarization parameters for copper in a 0.5 M H_2SO_4 solution in the absence and presence of various concentrations of MB at 298 K.

C (mM)	E_{corr} (mV/SCE)	I_{corr} ($\mu A\ cm^{-2}$)	β_c (mV dec^{-1})	β_a (mV dec^{-1})	η (%)
Blank	−49	50.3	−365	53	−
0.01	−64	25.6	−207	67	49.1
0.1	−79	19.1	−195	90	62.0
0.2	−103	12.5	−184	71	75.1
0.5	−57	8.6	−195	79	82.9
1	−88	5.1	−178	75	89.9

Based on extrapolation, some key data parameters, such as i_{corr}, E_{corr}, anodic, and cathodic Tafel slope (β_a and β_c) were given in Table 2. As shown in Table 2, the presence of MB caused the E_{corr} fluctuation of copper, but the change did not exceed 85 mV. Under the analysis combined with Fig. 4, it could conclude that MB was a mixed-type corrosion inhibitor [34]. Compared with the blank i_{corr} (50.3 $\mu A\ cm^{-2}$), the i_{corr} value of copper in 1 mM MB solution was dropped tenfold, only for 5.1$\mu A\ cm^{-2}$. This phenomenon suggested that MB could improve copper anti-corrosion by inhibiting its surface-active sites. In addition, the values of β_a and β_c did not change significantly, indicating the reaction mechanism of copper was not changed [35]. This was consistent with the above EIS results.

3.3 Weight loss

Weight loss was a specialized technique for evaluating the uniform corrosion rate of metals in corrosive media.

Figure 5. The weight loss data for copper in a 0.5 M H_2SO_4 solution in the absence and presence of various concentrations of MB at 298 K.

The obtained variation of weight loss data (*v*) on copper in 0.5 M H_2SO_4 containing various concentrations of MB was shown in Fig. 5. It should be noted that the corrosion rate of copper in blank 0.5 M H_2SO_4 was the highest and reached 215.3 mg m^{-2} h^{-1}. After copper was immersed in 0.5 M H_2SO_4 solution containing various concentrations of MB, the corrosion rate was significantly decreased. The smallest copper corrosion rate (28.9 mg m^{-2} h^{-1}) was obtained when the MB concentration was 1 mM. This result revealed that the MB film in the copper/solution interface inhibited the corrosion of copper.

3.4 SEM

Fig. 6 showed the SEM images of copper in 0.5 M H_2SO_4 solution containing 0 and 1 mM MB. As shown in Fig. 6a, copper was poor at resisting H_2SO_4 corrosion without the help of corrosion inhibitors. In the blank 0.5 M H_2SO_4 solution, the copper surface was covered with corrosion products and appeared uneven and rough. Unlike Fig. 6a, the surface of copper immersed in the solution containing 1 mM MB was smooth and flat, which only saw some polish scratches. This finding indicated that the MB film was critical to reducing the copper corrosion, which could effectively block contact between the copper and corrosive media.
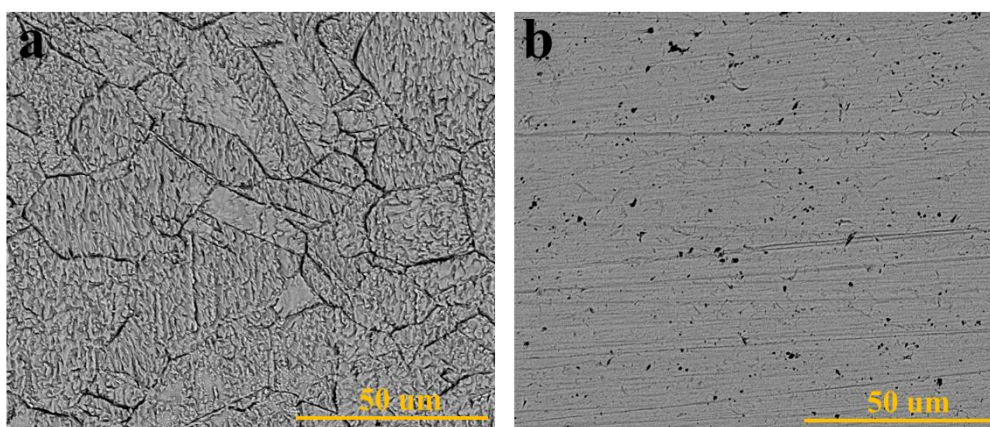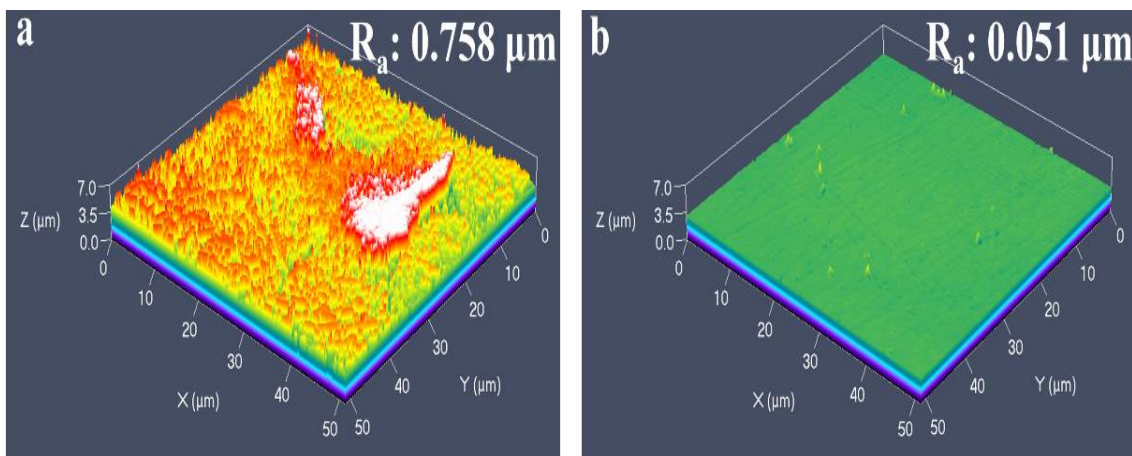

Figure 6. The SEM images of copper in 0.5 M H_2SO_4 solution containing 0 and 0.5 MM concentrations of MB at 298 K.

3.5 LSCM

Fig. 7 showed LSCM images of copper in 0.5 M H_2SO_4 solution containing different concentrations of MB (0 and 1 mM). It should be noted that the red color in this LSCM indicated severe corrosion. As shown in Fig. 7a, the entire copper surface was severely corroded, and many small hills were formed due to the accumulation of corrosion products. In addition, the surface roughness in the blank H_2SO_4 solution was the highest (Ra: 0.758 um). In contrast, the copper surface protected by 1 mM MB was flat with only a few tiny peaks. The surface roughness of copper in Fig. 7b was the lowest (Ra: 0.051 um). The considerable difference in Ra value in Figs 7a and b showed that the MB molecules

formed a protective barrier on the copper surface. In conclusion, the SEM and LSCM results were consistent with the above electrochemical and weight loss results, indicating that MB could provide high-efficiency protection for copper in 0.5 M H_2SO_4.

Figure 7. The LSCM images of copper in 0.5 M H_2SO_4 solution containing 0 and 0.5 MM concentrations of MB at 298 K.

3.6 Langmuir analysis

The adsorption mechanism of MB molecules on the copper surface was explored based on EIS data. As shown in Fig. 8, the R^2 value was 0.9988, close to 1. That was to say, Langmuir adsorption was the most suitable for explaining MB molecule adsorption on the copper surface. After referring to other works [36, 37], we calculated two important thermodynamic parameters (K_{ads} and ΔG^0_{ads}) according to the formula. The K_{ads} value (2.33×10^5 L/mol) in this work was much higher than in other reported work [38], indicating that MB was more easily adsorbed on the copper surface. The ΔG^0_{ads} value was between -20 kJ/mol ($\geq$ -20 kJ/mol, physical adsorption) and -40 kJ/mol ($\leq$ -40 kJ/mol, chemical adsorption) [39, 40], which showed that the adsorption of MB on the copper surface was dominated by chemical adsorption, while also existed physical adsorption. This high absolute value of ΔG^0_{ads} demonstrated a strong adsorptive affinity of inhibitor on the copper substrate [41].

$$R^2: 0.9988$$
$$K_{ads} (10^5 \text{ L/mol}): 2.33$$
$$\Delta G^0_{abs} (\text{kJ/mol}): -32.1$$
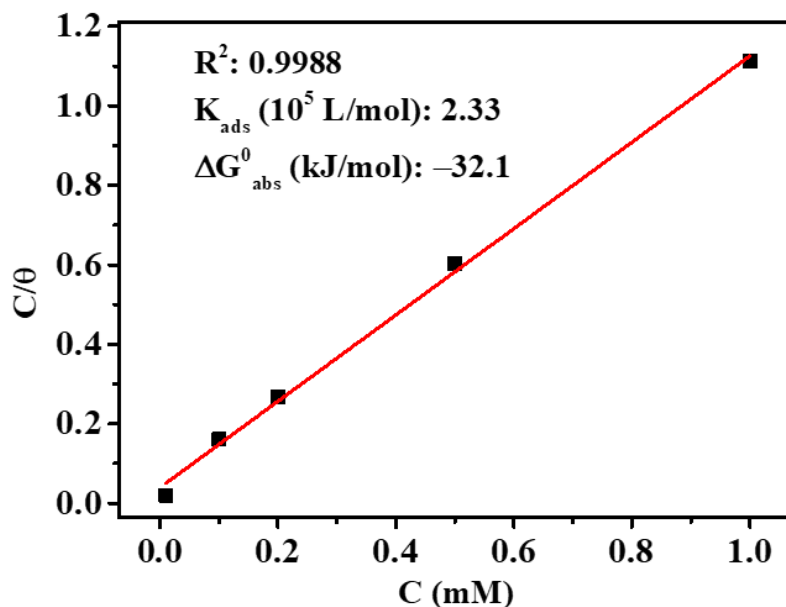
Figure 8. Langmuir adsorption isotherms and relevant thermodynamic parameters of investigated MB on the copper surface in a 0.5 M H_2SO_4 solution at 298 K.

3.7 Theoretical calculation

The adsorption analysis should first consider the inhibitor molecule's possible reaction sites. We conducted theoretical calculations to explore the interaction mechanism between MB molecule and copper surface.
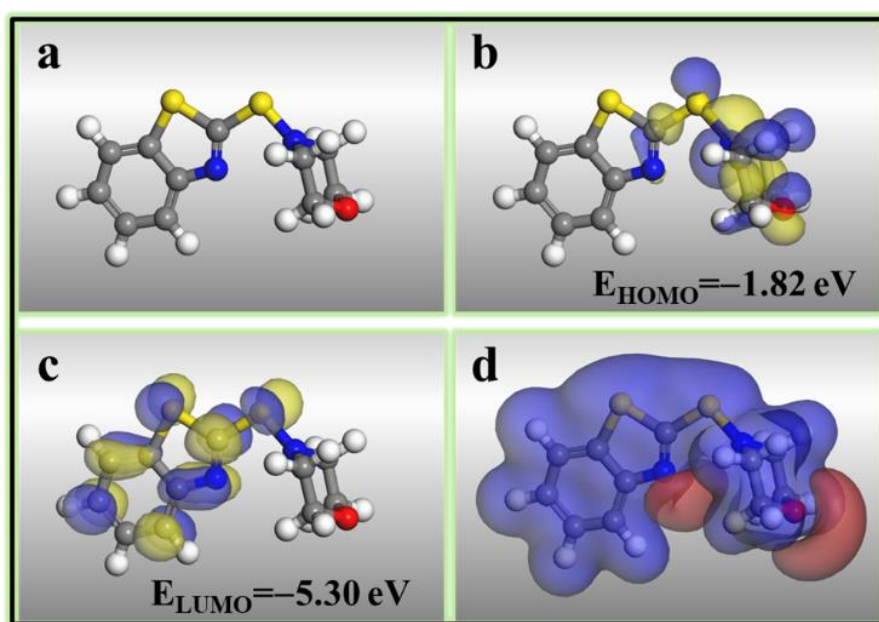
Figure 9. (a) Geometry optimization, (b) HOMO and (c) LUMO electron cloud distribution, (d) ESP map of MB molecule.

As shown in Fig. 9a, the MB molecule was almost in the same plane after geometry optimization, which was beneficial to parallel adsorption on the copper surface. Based on Figs 9b and c, it could be seen that HOMO and LUMO electron clouds were uniformly distributed on the MB molecule. That was to say, the benzene ring, heterocycle, and heteroatom could adsorb on the copper surface by gaining and losing electrons.

The E_{LUMO} and E_{HOMO} corresponded to electron-gaining and electron-donating capacities [42]. The lowest E_{LUMO} value displayed the highest electron-gaining performance, while the higher E_{HOMO} value meant a more vital electron-donating ability [43, 44]. As shown in Figs 9b and c, the E_{HOMO} value was -1.82 eV, the E_{LUMO} value was -5.30 eV, and thus the ΔE was 3.48 eV (E_{LUMO} -E_{HOMO}). Those results indicated that MB was more easily adsorbed to the copper surface and effectively inhibited copper corrosion, which was also consistent with the results of the ESP map (Fig. 9d).

4. CONCLUSIONS

In this work, we explored the anti-corrosion performance of MB for copper in 0.5 M H_2SO_4 solution based on a combination of experiments and theoretical calculations. The main results were concluded as follows.

1. MB could significantly improve copper R_f and R_{ct} value in 0.5 M H_2SO_4 solution, and the highest η value in EIS was 94%. The crucial reason was that MB could decrease the corrosion of copper in 0.5 M H_2SO_4 solution by forming a compact barrier film.

2. Based on the polarization curve results, it was found that MB was a mixed-type inhibitor, which could simultaneously reduce copper cathodic and anodic corrosion rates, especially when the MB concentration was 1 mM.

3. Combining the weight loss and morphology observations (SEM and LSCM), it intuitively demonstrated that the MB film could protect copper by blocking the active sites on the copper surface.

4. Langmuir adsorption and theoretical calculations appropriately demonstrated the interaction mechanism between MB molecule and copper surface at the thermodynamic and molecular levels. In short, MB exhibited admirable anti-corrosion ability by adsorbing on the copper surface in parallel with physical and chemical action.

References

1. Y. Qiang, S. Zhang, H. Zhao, B. Tan, and L. Wang, *Corrosion Science,* 161 (2019) 108193.
2. H. Li, S.T. Zhang, and Y.J. Qiang, *Journal of Molecular Liquids,* 321 (2021) 114450.
3. J.L. Zhang, and H. Li, *International Journal of Electrochemical Science,* 15 (2020) 5362-5372.
4. G. Zhang, L. Wu, A. Tang, Y. Ma, G.-L. Song, D. Zheng, B. Jiang, A. Atrens, and F. Pan, *Corrosion Science,* 139 (2018) 370-382.
5. H. Li, Y. Qiang, W. Zhao, and S. Zhang, *Corrosion Science,* 191 (2021) 109715.
6. M.J. Cui, J.D. Dong, K.H. Zhou, Y.H. Fang, J.B. Pu, H.C. Zhao, Y.G. Wang, and L.P. Wang, *International Journal of Electrochemical Science,* 13 (2018) 12010-12023.
7. Y. Zhang, Y. Qiang, H. Ren, J. Cao, L. Cui, Z. Zong, D. Chen, and T. Xiang, *Progress in Organic*

Coatings, 170 (2022) 106971.

8. B. Jiang, Q. Xiang, A. Atrens, J. Song, and F. Pan, *Corrosion Science,* 126 (2017) 374-380.
9. S. Eid, *International Journal of Electrochemical Science,* 16 (2021) 150852.
10. P.E. Alvarez, M.V. Fiori-Bimbi, A. Neske, S.A. Brandán, and C.A. Gervasi, *Journal of Industrial and Engineering Chemistry,* 58 (2018) 92-99.
11. S.Y. Chen, B. Zhu, and X. Liang, *International Journal of Electrochemical Science,* 15 (2020) 1-15.
12. Y. Qiang, H. Zhi, L. Guo, A. Fu, T. Xiang, and Y. Jin, *Journal of Molecular Liquids,* 351 (2022) 118638.
13. D.A. Winkler, M. Breedon, P. White, A.E. Hughes, E.D. Sapper, and I. Cole, *Corrosion Science,* 106 (2016) 229-235.
14. K.Y. Ann, H.S. Jung, H.S. Kim, S.S. Kim, and H.Y. Moon, *Cement and Concrete Research,* 36 (2006) 530-535.
15. Y. Qiang, L. Guo, H. Li, and X. Lan, *Chemical Engineering Journal,* 406 (2021) 126863.
16. C.M. Fernandes, L.X. Alvarez, N.E. dos Santos, A.C. Maldonado Barrios, and E.A. Ponzio, *Corrosion Science,* 149 (2019) 185-194.
17. P. Molaeipour, M. Ramezanzadeh, and B. Ramezanzadeh, *Bioelectrochemistry,* 143 (2022) 107970.
18. Y. Qiang, S. Zhang, S. Xu, and W. Li, *Journal of Colloid and Interface Science,* 472 (2016) 52-59.
19. Y. Qiang, S. Zhang, and L. Wang, *Applied Surface Science,* 492 (2019) 228-238.
20. B.X. Vuong, T.L. Huynh, T.Q.N. Tran, S.V.P. Vattikuti, T.D. Manh, P. Nguyen-Tri, A.T. Nguyen, P. Van Hien, and N. Nguyen Dang, *Materials Today Communications,* 31 (2022) 103641.
21. R. Álvarez-Bustamante, G. Negrón-Silva, M. Abreu-Quijano, H. Herrera-Hernández, M. Romero-Romo, A. Cuán, and M. Palomar-Pardavé, *Electrochimica Acta,* 54(23) (2009) 5393-5399.
22. Y. Qiang, H. Li, and X. Lan, *Journal of Materials Science & Technology,* 52 (2020) 63-71.
23. B. Tan, S. Zhang, Y. Qiang, W. Li, H. Liu, C. Xu, and S. Chen, *Journal of Molecular Liquids,* 286 (2019) 110891.
24. H. Li, Y.J. Qiang, W.J. Zhao, and S.T. Zhang, *Colloids and Surfaces a-Physicochemical and Engineering Aspects,* 616 (2021) 126077.
25. Y. Qiang, S. Zhang, S. Yan, X. Zou, and S. Chen, *Corrosion Science,* 126 (2017) 295-304.
26. M. Finšgar, and I. Milošev, *Materials and Corrosion,* 62(10) (2011) 956-966.
27. Y. Qiang, S. Zhang, B. Tan, and S. Chen, *Corrosion Science,* 133 (2018) 6-16.
28. H. Yang, W. Li, X. Liu, A. Liu, P. Hang, R. Ding, T. Li, Y. Zhang, W. Wang, and C. Xiong, *Construction and Building Materials,* 225 (2019) 90-98.
29. H. Li, S. Zhang, B. Tan, Y. Qiang, W. Li, S. Chen, and L. Guo, *Journal of Molecular Liquids,* 305 (2020) 112789.
30. G. Bahlakeh, B. Ramezanzadeh, A. Dehghani, and M. Ramezanzadeh, *Journal of Molecular Liquids,* 283 (2019) 174-195.
31. H. Tian, W. Li, A. Liu, X. Gao, P. Han, R. Ding, C. Yang, and D. Wang, *Corrosion Science,* 131 (2018) 1-16.
32. W. Zeng, W. Li, B. Tan, J. Liu, and J. Chen, *Journal of the Taiwan Institute of Chemical Engineers,* 128 (2021) 417-429.
33. B. Tan, S. Zhang, Y. Qiang, L. Guo, L. Feng, C. Liao, Y. Xu, and S. Chen, *Journal of Colloid and Interface Science,* 526 (2018) 268-280.
34. M.H. Shahini, M. Keramatinia, M. Ramezanzadeh, B. Ramezanzadeh, and G. Bahlakeh, *Journal of Molecular Liquids,* 342 (2021) 117570.
35. G. Cui, J. Guo, Y. Zhang, Q. Zhao, S. Fu, T. Han, S. Zhang, and Y. Wu, *Carbohydrate Polymers,* 203 (2019) 386-395.
36. L. Ma, Y. Qiang, and W. Zhao, *Chemical Engineering Journal,* 408 (2021) 127367.
37. B. Tan, B. Xiang, S. Zhang, Y. Qiang, L. Xu, S. Chen, and J. He, *Journal of Colloid and Interface Science,* 582 (2021) 918-931.
38. S.A. Umoren, M.M. Solomon, I.B. Obot, and R.K. Suleiman, *Journal of Industrial and Engineering*

Chemistry, 76 (2019) 91-115.

39. L.L. Liao, S. Mo, H.Q. Luo, and N.B. Li, *Journal of Colloid and Interface Science,* 520 (2018) 41-49.
40. M. Jokar, T.S. Farahani, and B. Ramezanzadeh, *Journal of the Taiwan Institute of Chemical Engineers,* 63 (2016) 436-452.
41. P. Mourya, S. Banerjee, R.B. Rastogi, and M.M. Singh, *Industrial & Engineering Chemistry Research,* 52(36) (2013) 12733-12747.
42. M. Oubaaqa, M. Ouakki, M. Rbaa, A.S. Abousalem, M. Maatallah, F. Benhiba, A. Jarid, M. Ebn Touhami, and A. Zarrouk, *Journal of Molecular Liquids,* 334 (2021) 116520.
43. D. Kumar, V. Jain, and B. Rai, *Corrosion Science,* 142 (2018) 102-109.
44. M. Ramezanzadeh, G. Bahlakeh, Z. Sanaei, and B. Ramezanzadeh, *Applied Surface Science,* 463 (2019) 1058-1077.